Distributed-Force Recovery for a Planar Photoelastic Tactile Sensor

R. E. Saad
Department of Electrical & Computer Engineering

A. Bonen
Department of Electrical & Computer Engineering

K. C. Smith
Department of Electrical & Computer Engineering

B. Benhabib
Department of Mechanical Engineering

Computer Integrated Manufacturing Laboratory, University of Toronto
5 King's College Road, Toronto, Ontario, Canada M5S 1A4
e-mail: beno@me.utoronto.ca

Abstract– **In this paper, a novel planar photoelastic tactile transducer is presented. A distributed force profile input to the transducer generates stress in the photoelastic layer of the transducer making it birefringent. Circularly-polarized input is elliptically polarized at the output due to phase-lead created in the stressed photoelastic layer. Our main objective is to recover the phase-lead distribution and correlate it to the input force profile. Since this distribution is a linear function of the force profile, the solution of the inverse tactile problem is significantly simplified. Herein, it is assumed that the light-intensity distribution can be detected by a CCD camera linked to an A/D converter.**

I. INTRODUCTION

The ability to sense and control parameters related to physical contact with the external environment is a fundamental part of the necessary sensory capabilities of future robots. Explorations of diverse technologies that can possibly be associated with tactile sensing have resulted in the utilizations of several forms of force transduction. Among the common methods of transduction are piezoelectric, piezoresistive, capacitive and optical. Extensive surveys of robotic-tactile-transduction technologies, providing considerable details of the performance of each of these types of tactile sensors, have been presented in [1-3].

Photoelasticity, in the context of tactile sensing, is among the optical phenomena that has received little attention in the literature. The few studies that have been published include: an introduction to photoelastic tactile sensing [4], the description of photoelastic slippage sensors [5,6], and a theoretical analysis of a photoelastic tactile transducer developed in our laboratory [7].

In a photoelastic transducer, the illumination of the transducer is typically achieved using a polaridoscope [8]. The output light-intensity distribution of the polaridoscope is created by the birefringence induced in the photoelastic element when forces are applied to the transducer. The birefringence creates a phase-lead distribution that modulates the output light-intensity [9]. The phase-lead distribution, as will be shown in Section III, is a linear function of the force profile, simplifying the solution of the inverse tactile problem (that is, the recovery of the force profile).

A novel algorithm that recovers the phase-lead distribution was first introduced in [7] for the case of a noise-free (ideal) light-intensity distribution. Herein, the non-ideal case is addressed. It is assumed that the light-intensity is detected by a CCD camera linked to an A/D converter. Both elements introduce electronic noise, and the A/D converter adds quantization error to the detected light-intensity distribution.

In this paper, an algorithm that accurately and effectively determines the phase-lead distribution from a noisy light-intensity distribution is presented. The model used to simulate the transducer is based on a simple 2-D opto-mechanical model previously reported in [4] and adopted for our transducer. The model allows the formation of closed-form equations for both the light-intensity distribution and for the phase-lead distribution.

II. THE TRANSDUCER

The proposed transducer consists of a simply-supported two-layer beam, with a mirrored surface between the two layers, Fig. 1. In our analysis, it is assumed that normal line-distributed forces are applied to part of the top surface of the beam, separated by equal distances, *s*, from each other. The area covered by these lines is referred to as the force-application region. The upper layer is added to protect the rear surface of the mirror. For simplicity, it is assumed that this layer has the same mechanical properties as the lower photoelastic layer (with the same modulus of elasticity and Poisson's coefficient).

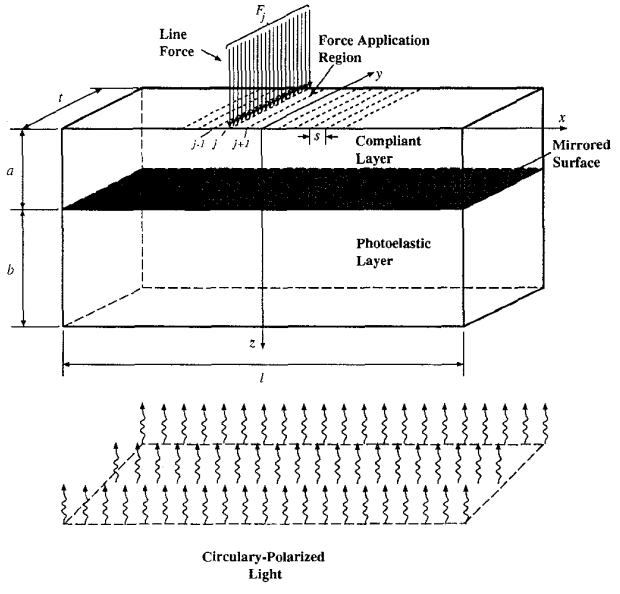

Fig. 1. Two-layer photoelastic transducer.

0-7803-2615-6/95/$4.00 © 1995 IEEE

Circularly-polarized monochromatic light illuminates the bottom surface of the transducer. A circular-reflection polaridoscope is used for this purpose [4,8]. The light propagates parallel to the z-axis, passes through the photoelastic material, reflects from the mirror and returns through the photoelastic material. If no force is applied onto the transducer, the returning light is circularly polarized since the photoelastic material is isotropic. If a force profile is applied, stresses are induced in the photoelastic layer making the material birefringent. This introduces a certain phase-difference (a phase-lead) between the components of the electric field associated with the light-wave propagation in the two allowed directions of polarization [9]. The two directions of polarization are in the plane perpendicular to the direction of propagation, in our case the x-y plane. As a consequence of this effect, the output light is elliptically polarized creating a phase-lead distribution, p, between the input light and the output-light at each point on the x-y plane.

III. PHASE-LEAD DISTRIBUTION

The normalized output-light-intensity distribution, $I(x,y)$, at the output of the circular-reflection polaridoscope is given by, [4]:

$$I(x,y) = \sin^2 \frac{p(x,y)}{2} . \quad (1)$$

To calculate the phase-lead distribution, it is assumed that the distribution of stresses is given by the plane-stress approximation described in [3,4]. This model allows us to analyze the behavior of the transducer using closed-form equations, where the phase-lead is only a function of x. The total phase-lead is the summation (integral) of all the phase-leads introduced at different points of the photoelastic layer along the z-coordinate.

Let F_j , shown in Fig. 1, be the magnitude of the force applied at the j^{th} (discrete) position (tactel) in the force-application region, then, the phase-lead distribution, p_j , can be calculated as:

$$p_j(x) = \frac{4K_{ss}}{\lambda t}\left[\frac{a^2}{(x-x_j)^2+a^2} - \frac{b^2}{(x-x_j)^2+b^2}\right]F_j , \quad (2)$$

where K_{ss} is the stress optical coefficient, t is the width of the photoelastic sensor, a is the thickness of the non-photoelastic upper layer, b is the thickness of the photoelastic lower layer, x_j is the x-coordinate of the j^{th} tactel and λ is the wavelength of the input light.

For a set of forces applied at n tactels, the total phase-lead distribution is given by [7]:

$$p(x) = \sum_{j=1}^{n} p_j(x) = \sum_{j=1}^{n} \psi_j(x)\, F_j , \quad (3)$$

where

$$\psi_j(x) = \frac{4K_{ss}}{\lambda t}\left[\frac{a^2}{(x-x_j)^2+a^2} - \frac{b^2}{(x-x_j)^2+b^2}\right] . \quad (4)$$

Equation (3) is obtained by applying the principle of superposition. As a consequence, the phase-lead distribution is a linear function of the applied forces.

The normalized-intensity distribution at the output of the polaridoscope is given by:

$$I(x) = \sin^2 \frac{p(x)}{2} . \quad (5)$$

In [7], an algorithm to recover $p(x)$ from $I(x)$ was introduced. One can note that the major problem that exists in inverting (5) is the possibility that $p(x) \le -\pi$ for some $-l/2 \le x \le l/2$.

The first step in the algorithm is the classification of the critical points of $I(x)$ as follows:

(a) *Class 1*: critical points of $I(x)$, where $I(x)$=1 and the first non-negative derivative is of the form $d^{2k+1}I/dx^{2k+1}$ for some integer $k \ge 1$.

(b) *Class 2*: critical points of $I(x)$, where $I(x)$=0 and the first non-negative derivative is of the form $d^{2k+1}I/dx^{2k+1}$ for some integer $k \ge 1$.

(c) *Class 3:* critical points of $I(x)$, which are local extrema but do not satisfy conditions (a) or (b).

The second step in the algorithm deals with the recovery of the phase-lead distribution. If it is assumed that $p(l/2) \ge -\pi$ the phase-lead distribution can be reconstructed using the following formula:

$$p(x) = -2\pi M - (-1)^{M+N} 2 \arcsin\sqrt{I(x)} , \quad (6)$$

where $M \rightarrow M + (-1)^K$.

The algorithm starts with M=0, N=0, and K=0. The phase-lead distribution is recovered point-by-point increasing x from $-l/2$ to $l/2$. When a *Class 3* critical point is encountered, K is increased by one; when a *Class 2* critical point is encountered, N is increased by one; and, when a *Class 1* critical point is encountered, M is increased or decreased by one depending on the value of K.

IV. NOISE AND QUANTIZATION ERROR

It is assumed that light originating from the polaridoscope is detected by a CCD linear array with an active length equal to the length of the transducer and set parallel to the x coordinate. Since the linear array samples the light-intensity distribution in pixel-quantized space, Equation (5) can be re-written in a discrete form as:

$$I(x_i) = \sin \frac{p(x_i)}{2} \qquad \text{for } i=1,2,...m, \quad (7)$$

where m is the number of pixels of the linear array.

The equations for $p(x)$ and $\psi_j(x)$, (3) and (4) respectively, can also be re-written in a discrete form as:

$$P_i = p(x_i) \qquad \text{for } i=1,2,...m, \quad (8)$$

$$\psi_{ij} = \psi_j(x_i) \qquad \text{for } i=1,2..m \text{ ; } j=1,2...n . \quad (9)$$

The discrete version of (3) can, thus, be re-written using a matrix notation as:

$$\boldsymbol{P} = \Psi \boldsymbol{F}, \tag{10}$$

where

$$\boldsymbol{P} = \begin{bmatrix} P_1 \\ P_2 \\ \vdots \\ P_m \end{bmatrix}; \Psi = \begin{bmatrix} \psi_{11} & \psi_{12} \cdots \psi_{1n} \\ \psi_{21} & \psi_{22} \cdots \psi_{2n} \\ \vdots & \vdots \quad \vdots \\ \psi_{m1} & \psi_{m2} \cdots \psi_{mn} \end{bmatrix}; \boldsymbol{F} = \begin{bmatrix} F_1 \\ F_2 \\ \vdots \\ F_n \end{bmatrix}. \tag{11}$$

Here, $\boldsymbol{P}$ is the phase-lead vector, Ψ is the base matrix, and $\boldsymbol{F}$ is the input force-profile vector. A relation similar to (10), but between strains and forces, was reported in [10-12] for the case of piezo-resistive tactile transducers.

Once the light-intensity has been discretized by the linear array, the measurements are converted into digital form by an A/D converter. The A/D converter introduces quantization error in addition to the random electronic noise that would be present due to the detection process. The detected light-intensity distribution (in grey levels), I_d, can be written as:

$$I_d(x_i) = round\left[A \sin^2 \frac{p(x_i)}{2} + n_o(x_i) + I_o \right] \text{ for } i=1,2...m, \tag{12}$$

where n_o is the total noise introduced into the measurement; I_o is the minimum average voltage applied to the A/D converter, such that $I_o + \min(n_o) \geq 0$; and A is the maximum allowed dynamic range of the A/D converter, such that $A + I_o + \max(n_o) \leq 2^B - 1$, (where B is the number of bits in the A/D converter). The function $round(\cdot)$ returns the closest integer to the real number $(\cdot)$.

Now, the phase-lead distribution has to be recovered from (8). However, the critical points of I_d cannot be classified using the algorithm outlined in Section III since the derivatives of I_d would be zero or infinite. Thus, a modified algorithm that allows us to recover the phase-lead distribution from a noisy light-intensity distribution is reported in the next section.

V. RECOVERING THE PHASE-LEAD FROM NOISY DATA

The proposed algorithm is explained herein via an example. Let the light-intensity distribution be given by (12), and $p(x_i)$ be calculated using (10). For the example, the parameters and dimensions of the transducer, the A/D converter and the linear array are as follows: a=0.5mm, b=3mm, t=2mm, l=250mm, s=1mm, λ=632.8nm, E=0.0046GPa, K_{ss}=2.93x10^{-9}m^2/N, ν=0.5, B=8 bits, m=2048, n=11, I_o=5 and A=245. The noise n_o is assumed to be random and limited between -5 and 5 grey levels.

The base matrix Ψ of the system is calculated using (4), (9) and (11). For the example, it is assumed that each tactel of the transducer is subjected to the same force, namely F_j=0.1N for j=1,2...11. Fig. 2 shows the noisy light-intensity distribution corresponding to the phase-lead distribution shown in Fig. 3.

The first step in the modified algorithm is to filter the light-intensity distribution shown in Fig. 2 with an ideal low-pass filter, whose pass-band is 10 μm^{-1}. Using it, the noise is reduced approximately to the range of -2 to 2 grey levels, from -5 to 5. The normalized filtered light-intensity distribution is shown in Fig. 4. As well, Fig. 4 indicates the 25 critical points c_k, k=1,2...25.

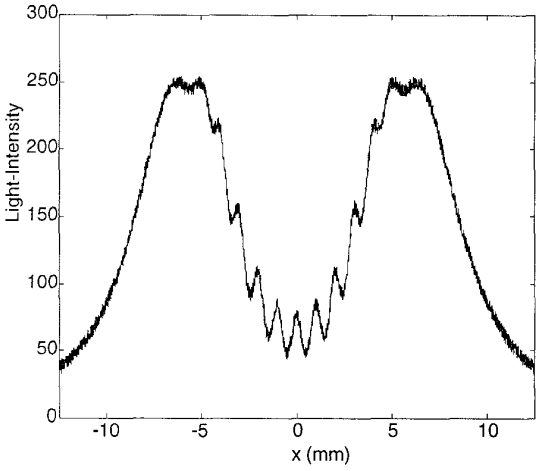

Fig. 2. Detected light-intensity distribution in grey levels.

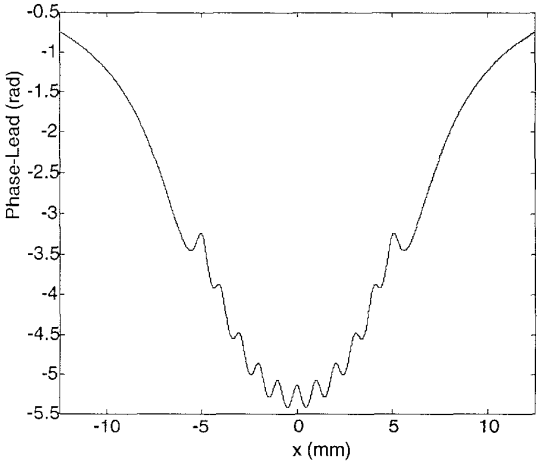

Fig. 3. Phase-lead distribution.

The algorithm verifies that two consecutive critical points do not occur too close to each other since such closely-paired critical points would imply a noisy observation. The threshold value for closeness was chosen as 20 pixels herein.

The next step in the algorithm is defining three regions in the normalized light-intensity distribution, as shown in Fig. 4, for the classification of the critical points. On the normalized intensity scale, Region 1 is defined as $0.98 \leq I \leq 1$, Region 2 as $0 < I < 0.02$ and Region 3 as $0.02 \leq I \leq 0.98$. The widths of Regions 1 and 2 were obtained approximately by dividing the maximum error in the filtered light-intensity distribution by A (that is, 4/245~0.02).

The critical points are now classified as follows:

(a) All *local extrema* in Region 1 are either *Class 1* or *Class 3* points (following the classification used in Section III). In our example, c_1, c_2, c_3, c_{23} and c_{25} are in Region 1.

(b) All *local extrema* in Region 2 are either *Class 2* or *Class 3* points. In our example, there are no critical points in Region 2.

(c) All *local extrema* in Region 3 are *Class 3* points. In our example, c_k for k=4,5...22 and c_{24} are in Region 3.

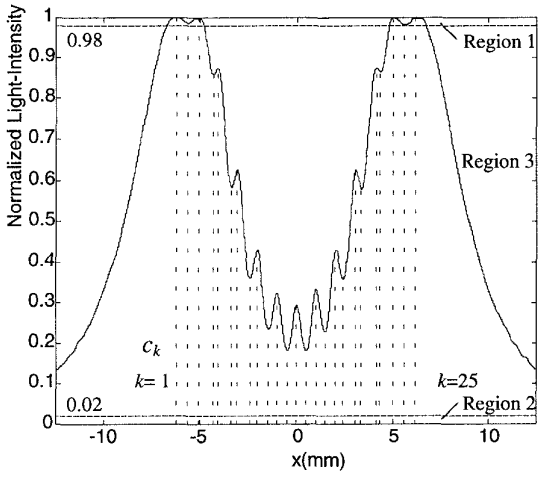

Fig. 4. Normalized light-intensity distribution.

Due to uncertainty about the class of critical points in Regions 1 and 3, several different phase-lead distributions can be recovered using (6), based on the algorithm outlined in Section III, of which only one is correct. Each local extremum in Regions 1 and 2 would yield two possible phase-lead distributions. If the total number of local extrema in Regions 1 and 2 is C, then the total number of possible phase-lead distribution is 2^C. In our example C=5, leading to 32 possible phase-lead distributions.

The next step in the algorithm tries to minimize the number of possible phase-lead distributions. To accomplish this objective, all the possible cases are checked with respect to a set of verification rules:

Rule 1: If c_{k1} and c_{k2} are both *Class 1* or both two *Class 2* points such that between them only *Class 3* critical points exit, then the number of Class 3 critical points must be odd. For instance, in our example, if c_1 and c_3 are both *Class 1* type, then c_2 must be a *Class 3* type.

Rule 2: If c_{k1} is a *Class 1* (*Class 2*) point and c_{k2} is *Class 2* (*Class 1*) point such that between them only *Class 3* critical points exist, then the number of *Class 3* critical points must be even. In our example, this rule does not apply since there are no critical points in Region 2.

Rule 3: The transducer is geometrically symmetric and operates in a range of forces such that the following boundary conditions apply: $p(-l/2) \geq -\pi$ and $p(l/2) \geq -\pi$. This implies that the parameter M in (6), for $x = -l/2$ and $x = l/2$, must be zero. For instance, in our example, if c_1 is a *Class 1* point, and the rest of the critical points are *Class 3* type, with M=0 for $x = -l/2$, and M=1 for $x = l/2$, then this case does not satisfy this rule and must be eliminated.

Applying the above verification rules to the set of 32 possible cases in our example, the possible set of phase-lead distributions was reduced to 8.

The next step in the algorithm is reconstructing the phase-lead distribution for the reduced set at hand. In our example, if we assign the number "1" to *Class 1*, "-1" to *Class 2* and "0" to *Class 3*, the 8 possible cases can be described as in Table I.

TABLE I. REDUCED SET OF POSSIBLE CRITICAL POINTS.

Case #	c_1	c_2	c_3	c_k (k=4,5...22)	c_{23}	c_{24}	c_{25}
1	0	0	0	0	0	0	0
2	0	0	0	0	1	0	1
3	0	0	1	0	0	0	1
4	0	0	1	0	1	0	0
5	1	0	0	0	0	0	1
6	1	0	0	0	1	0	0
7	1	0	1	0	0	0	0
8	1	0	1	0	1	0	1

For each case shown in Table I, the phase-lead distribution is recovered using the "*ideal*" algorithm described in Section III. As an example, the recovered phase-lead distribution for Case 1 is shown in Fig. 5. As can be seen, when compared with the true input phase-lead distribution of Fig. 3, this guessed phase-lead distribution is obviously not the correct one (although we would not know that during run-time since the true phase-lead distribution would not be known).

The next step in the algorithm, thus, is finding a method to eliminate the wrong phase-lead distributions appearing in Table I.

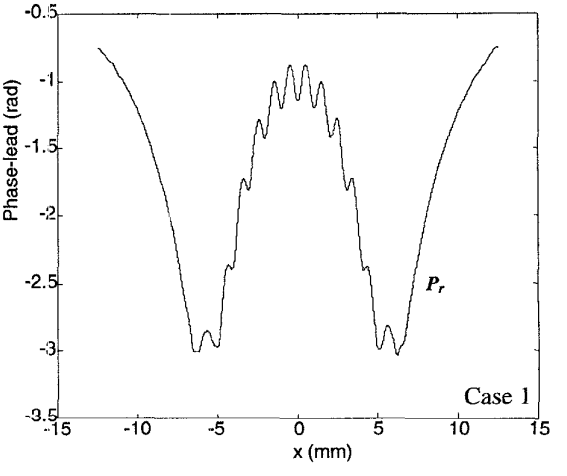

Fig. 5. Recovered phase-lead distribution for Case 1.

To achieve the above objectives, the force-profiles corresponding to the limited set of potential phase-lead distributions must be found by solving (10). The discretized inverse problem consists of finding the specific force-profile vector, $\boldsymbol{F}_r$, given the specific phase-lead vector $\boldsymbol{P}_r$ and Ψ. A similar problem has been addressed in a previous study for the case of a piezoresistive tactile sensor, [11]. Therein, it was shown that the inverse-tactile problem is ill-posed, and needs normalization. In the same work, a neural network was proposed to solve the inverse-tactile problem. In our case, we decided to use a simple optimization function which can be found in the Optimization Toolbox of Matlab, to solve the inverse problem,

$$\boldsymbol{F}_r = \text{nnls}(\Psi, \boldsymbol{P}_r) \ . \qquad (13)$$

Equation (13) solves the non-negative least-squares (nnls) problem stated as

$$\min_{F_r} \| \Psi \ \boldsymbol{F}_r - \boldsymbol{P}_r \| \ , \qquad \text{such that } \boldsymbol{F}_r \geq 0, \qquad (14)$$

where Ψ and $\boldsymbol{F}_r$ are the coefficients of the objective function. The vector $\boldsymbol{F}_r$ is restricted to be non-negative due to the positive force profile requirement in our case.

For Case 1 in Table I, the following force profile was recovered using (13):

$\boldsymbol{F}_r$ =(0.2156, 0.0868, 0, 0, 0, 0, 0, 0, 0, 0.0860, 0.2161) N.

The recovered force profile obtained by (13) must be verified via (10). Let $\boldsymbol{P}_v$ be the phase-lead distribution obtained when the estimated force profile $\boldsymbol{F}_r$ is applied to (10):

$$\boldsymbol{P}_v = \Psi \ \boldsymbol{F}_r \ . \qquad (15)$$

For the correct guess of $\boldsymbol{P}_r$ the difference between $\boldsymbol{P}_r$ and $\boldsymbol{P}_v$ must be minimal due to the least squares fit.

In Fig. 6, both $\boldsymbol{P}_r$ and $\boldsymbol{P}_v$ are plotted. As can be observed, there exists a large difference between the two phase-lead distributions. This correctly implies that Case 1 is not the true phase-lead distribution.

For Case 4, the corresponding $\boldsymbol{P}_r$ and $\boldsymbol{P}_v$ are shown in Fig. 7. Once again, it is noted that Case 2 is not the true phase-lead distribution.

The procedure is repeated for all the cases of Table I. The correct recovered phase-lead distribution is the one that best matches the associated phase-lead distribution $\boldsymbol{P}_v$, namely the one that provides the minimum of a normalized error defined, for each case, as:

$$Error(\%) = \frac{1}{\Delta P_{max}} \max\{abs[\boldsymbol{P}_v - \boldsymbol{P}_r]\} \times 100, \qquad (16)$$

where the function *abs* calculate the absolute value of each component of the difference between $\boldsymbol{P}_r$ and $\boldsymbol{P}_v$ and ΔP_{max} is the difference between the overall absolute maximum and the overall absolute minimum of $\boldsymbol{P}_r$ and $\boldsymbol{P}_v$.

For the example under analysis, the correct phase-lead distribution is the one that corresponds to Case 5, Fig. 8. As can be seen, $\boldsymbol{P}_r$ and $\boldsymbol{P}_v$ are almost identical. The normalized error for this case is 3.2%. The next smallest error percentage

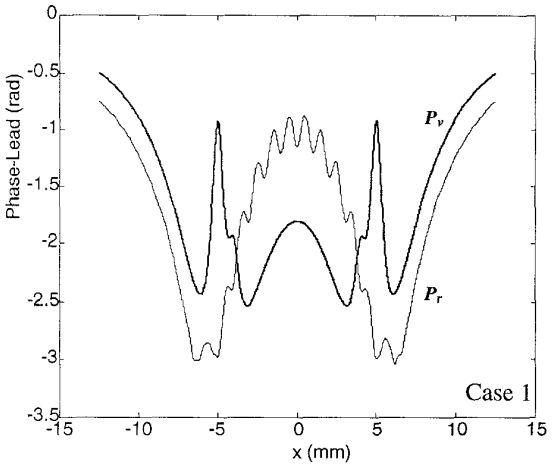

Fig. 6. Phase-lead distributions P_r and P_v for Case 1.

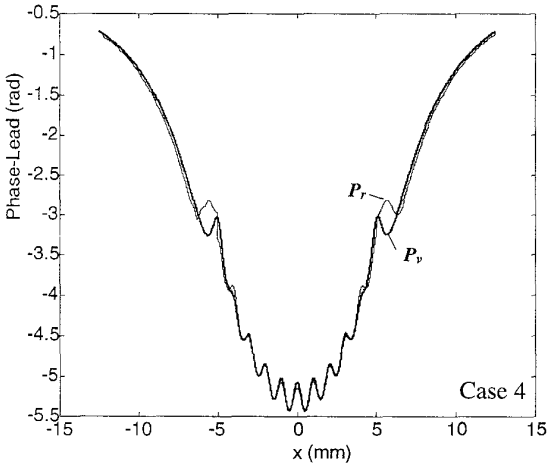

Fig. 7. Phase-lead distributions $\boldsymbol{P}_v$ and $\boldsymbol{P}_r$ for Case 4.

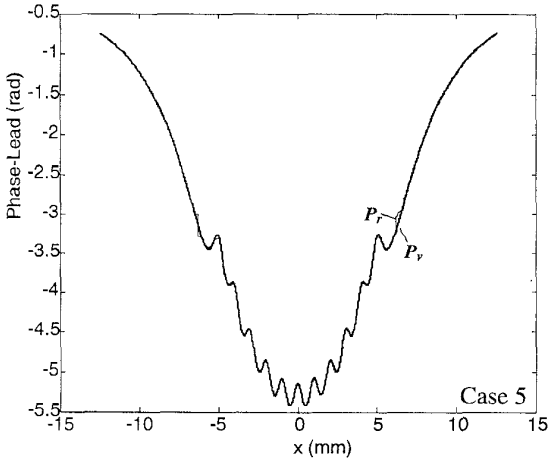

Fig. 8. Correct phase-lead distributions $\boldsymbol{P}_v$ and $\boldsymbol{P}_r$.

was for Case 4, 9.4%, as shown in Table II, where the normalized error for each case has been calculated.

TABLE II. NORMALIZED ERROR FOR EACH CASE SHOWN IN TALE I.

Case #	1	2	3	4	5	6	7	8
Error(%)	42.9	40.6	9.6	9.4	3.2	10.1	40.9	40.6

The recovered force profile for Case 5 is:

$$\boldsymbol{F}_r = (0.0994, 0.1017, 0.1004, 0.1002, 0.0987, 0.0994, 0.0996, 0.1006, 0.1011, 0.1019, 0.0972)\ \mathrm{N}.$$

When one compares the above $\boldsymbol{F}_r$ with the true input F_j=0.1N, j=1,2...11, the maximum error in force recovery is determined as 1.9%.

CONCLUSIONS

In this paper, a general algorithm has been presented for the automatic recovery of the phase-lead distribution for a photoelastic tactile sensor. The noisy light-intensity distribution is assumed to be detected by a linear array CCD camera linked to an A/D converter. The algorithm takes into account the random noise generated by the electronic circuits of the camera, as well as the quantization error generated by the A/D converter.

Simulations using a two-dimensional opto-mechanical model were presented to verify the proposed algorithm. To solve the inverse tactile problem an optimization function was successfully implemented

In practice, finding the correct phase-lead distribution might in some cases be computationally time-consuming if carried out sequentially. Particularly because of the complexity of the algorithm by which the inverse tactile problem is solved. However, there is no restriction on processing the different phase-lead distributions in a parallel manner. Use of dedicated hardware to solve the inverse tactile problem, as the one proposed in [11] for instance, is particularly attractive.

ACKNOWLEDGMENT

The authors are grateful for the financial support provided by the Natural Sciences and Engineering Research Council of Canada. Mr. Saad would also like to thank CNPq, Brazil, for its financial support.

REFERENCES

[1] H. R. Nicholls and M. H. Lee, "A Survey of Robot Tactile Sensing Technology," *The International Journal of Robotics Research*, Vol. 8, No. 3, 1989, pp. 3-30.

[2] R. A. Russell, *Robot Tactile Sensing*, Prentice Hall, Brunswick, 1990.

[3] Ed. H.R. Nicholls, *Advanced Tactile Sensing for Robotics*, World Scientific Publishing Co. Pte. Ltd., Singapore, 1992.

[4] A. Cameron, R. Daniel and H. Durrant-Whyte, "Touch and Motion," *IEEE, International Conference on Robotics and Automation*, Philadelphia, 1988, pp. 1062-1067.

[5] F. Eghtedari and C. Morgan, "A Novel Tactile Sensor for Robot Applications", *Robotica*, Vol. 7, 1989, pp. 289-295.

[6] S. H. Hopkins, F. Eghtedari and D. T. Pham, "Algorithms for Processing Data from a Photoelastic Slip Sensor," *Mechatronics*, Vol. 2, No. 1, 1992, pp. 15-28.

[7] R. E. Saad, B. Benhabib and K. C. Smith, "A Novel Photoelastic Tactile Transducer for Robotics", *SME, Fifth World Conference on Robotics Research*, Cambridge, Massachussetts, 1994, pp. 4-1:14.

[8] P. S. Theocaris and E. E. Gdoutos, *Matrix Theory of Photoelasticity*, Springer-Verlag, Berlin, 1979.

[9] K. Iizuka, *Engineering Optics*, Springer-Verlag, 2nd Ed., Germany, 1987.

[10] R. S. Fearing and J. M. Hollerbach, "Basic Solid Mechanics for Tactile Sensing," *International Journal of Robotics Research*, Vol. 4, No. 3, pp. 40-54.

[11] Y. C. Pati, *Neural Networks for Low Level Processing of Tactile Sensory Data*, Master's Thesis, Department of Electrical and Computer Engineering, University of Maryland, College Park, 1989.

[12] R. E. Ellis, S. R. Ganeshan and S. J. Lederman, "A Tactile Sensor Based on Thin-Plate Deformation," Robotica, Vol. 12, 1994, pp. 343-351.